QUANTUM MELTING ON A LATTICE AND DELOCALIZATION TRANSITION

by

Eugene V. Tsiper

A dissertation submitted to the faculty of
The University of Utah
in partial fulfillment of the requirements for the degree of

Doctor of Philosophy

Department of Physics

The University of Utah

August 1997

THE UNIVERSITY OF UTAH GRADUATE SCHOOL

SUPERVISORY COMMITTEE APPROVAL

of a dissertation submitted by

Eugene V. Tsiper

This dissertation has been read by each member of the following supervisory committee and by majority vote has been found to be satisfactory.

	Chair: Alexei L. Efros
	Yong-Shi Wu
	Bill Sutherland
	John Worlock
	Kenneth Golden

THE UNIVERSITY OF UTAH GRADUATE SCHOOL

FINAL READING APPROVAL

To the Graduate Council of the University of Utah:

I have read the dissertation of Eugene V. Tsiper in its final form and have found that (1) its format, citations, and bibliographic style are consistent and acceptable; (2) its illustrative materials including figures, tables, and charts are in place; and (3) the final manuscript is satisfactory to the Supervisory Committee and is ready for submission to The Graduate School.

Date

Alexei L. Efros
Chair, Supervisory Committee

Approved for the Major Department

P. Craig Taylor
Chair/Dean

Approved for the Graduate Council

Ann W. Hart
Dean of The Graduate School

ABSTRACT

Quantum melting of a lattice Wigner crystal and the insulator-metal transition assosiated with it are studied using numerical techniques. It is shown that the lowest in energy excited state of the system plays crucial role in quantum melting. In a large enough system this state is a point defect in a Wigner crystal. Based on numerical data a simple picture of the transition is proposed. This picture leads to an empirical criterion that allows estimation of the critical point of the transition in various cases. It is shown that the picture provides a good description of the phase diagram of quantum melting in the one-dimensional (1D) model with the nearest- and the next-nearest interactions in the regions where the mixing of two competing crystals is not important. In the region of strong mixing an interesting metallic phase of a strongly interacting system is found.

To M. P. T. & $\mathcal{M}$.

CONTENTS

LIST OF FIGURES

ACKNOWLEDGEMENTS

I would like to express my sincere gratitude to Professor Alexei Efros for his continuous guidance and support, and for the wonderful physics he gave me a chance to be involved in.

It is my pleasure to acknowledge innumerous exciting and instructive conversations with Professor Emmanuel Rashba.

I would like to thank Professors Daniel Mattis, John Worlock, Bill Sutherland, Yong-Shi Wu, and Mikhail Raikh for a lot of helpful discussions in the course of my study.

CHAPTER 1

INTRODUCTION

The problem of the insulator-metal transition and the role of electron-electron interaction in this transition is a focus of modern condensed matter physics. It has been shown[1, 2, 3] that in the systems with strong disorder the interaction is in favor of delocalization because electrons may help each other to overcome the random potential. In clean systems the role of the interaction is the opposite. It is well known that when the interaction is strong enough, electrons behave classically and form a periodic structure called Wigner crystal. In such structures each electron is localized in a potential well created by all other electrons.

The Wigner crystal in continuum is not formally a dielectric, since it can move as a whole and carry current. However, due to the presence of shear modulus it can be pinned by small disorder. In contrast to the continuum case, the Wigner crystal on a lattice is a dielectric without any disorder. It does not have any sound or plasma modes and its excitation spectrum has a gap.

The Wigner crystal melts with increasing temperature. At zero temperature it becomes unstable (melts) when the average kinetic energy of the particles becomes larger than characteristic interaction strength. We shall refer to a phase transition that occurs at zero temperature as a result of variation of some parameter in Hamiltonian as *quantum* phase transition.

Because of the dielectric nature of the Wigner crystal, its melting can be connected to the insulator-metal transition. The ground-state energy of the continuum Wigner crystal and its zero-temperature melting has been widely studied in the recent years both with and without a magnetic field[4]. The insulator-metal transition that occurs due to the melting of the lattice Wigner crystal is the subject of the present work.

The great majority of the efforts made recently to study correlated particles on a lattice were restricted to the Hubbard model or $t - J$ model which are believed to be related to high-T_c superconductivity (see review [5]). These models exhibit metal-insulator

transitions, but no Wigner crystallization, since the long-range part of the interaction is missing.

The goal of the present work is to study quantum melting of the Wigner crystal on a two-dimensional (2D) square lattice and the insulator-metal transition associated with it. Some 1D examples are also studied in Chapter IV. A system of spinless fermions is considered with the following model Hamiltonian:

$$H = J \sum_{\mathbf{r},\mathbf{s}} a^{\dagger}_{\mathbf{r}+\mathbf{s}} a_{\mathbf{r}} + \frac{1}{2} \sum_{\mathbf{r} \neq \mathbf{r}'} n_{\mathbf{r}} n_{\mathbf{r}'} V(\mathbf{r} - \mathbf{r}'). \tag{1.1}$$

Here $a_{\mathbf{r}}$ and $a^{\dagger}_{\mathbf{r}}$ are the fermionic creation and annihilation operators, $n_{\mathbf{r}} = a^{\dagger}_{\mathbf{r}} a_{\mathbf{r}}$, and the summation is performed over the lattice sites $\mathbf{r}$, $\mathbf{r}'$ and over the vectors of translations to the nearest-neighbor sites, $\mathbf{s}$.

In 2D and 3D the Hamiltonian Eq. 1.1 with short range and long range interaction has been mostly considered for bosons. The 3D Hamiltonian Eq. 1.1 for hard-core bosons was first introduced to describe approximately some properties of He^4, taking into account the hardcore constraint[6]. An equivalent spin version of the bosonic Hamiltonian with nearest-neighbor interaction has been studied extensively due to its importance in magnetic problems. Much attention to the bosonic system has been paid recently due to experiments on superconductor-insulator transition found in thin superconducting films[7, 8, 9, 10]. In these systems supersolid and superfluid phases have been found.

The Hamiltonian Eq. 1.1 has been extensively studied in 1D. In this case the Hamiltonians for spinless fermions and for the hard-core bosons are equivalent. It is easy to see that for an odd number of particles the Hamiltonians matrices are identical. For an even number of particles the problem with antiperiodic boundary conditions is equivalent to the bosonic problem with periodic conditions and vice versa.

The 1D problem with the nearest-neighbor interaction at half filling is exactly soluble[11, 12, 13]. This instructive problem shows that the transition is not of the first order and that the insulator-metal transition appears at the same point as the structural transition[13].

Surprisingly, almost no works exist on the fermionic version of the Hamiltonian Eq. 1.1 in 2D and 3D. Pikus and Efros[14] have performed a computer modeling for 2D Hamiltonian Eq. 1.1 with Coulomb interaction on a square lattice at filling factors $\nu = 1/3$ and $1/6$ in a cluster 6×6. They have suggested that the lifting of the ground-state degeneracy with increasing J is a very good diagnostic of the structural phase transition.

In this work the Hamiltonian Eq. 1.1 with different types of interaction potential is studied numerically. Based on comparison of the numerical data for long-range and short-range interaction, we propose a simple picture of the transition. This picture leads to an empirical criterion for estimation of the critical point.

The exact diagonalization technique is used to study finite clusters up to 16 electrons. It has been preferred to the quantum Monte-Carlo technique because the latter is suitable for calculating the properties of the ground state only. Also, the quantum Monte-Carlo technique applied to fermi systems suffers from the so-called sign problem[5].

We detect the structural transition by studying the ground-state splitting as suggested by Pikus and Efros[14]. Simultaneously the sensitivity of the spectrum to boundary conditions is computed as a criterion of the insulator-metal transition[15, 16].

The thesis is organized as follows. In Chapter 2 the persistent current of a 2D system of free fermions is studied. This is important since the amplitude of the persistent current is used as a criterion of delocalization. It is shown that in 2D rectangular clusters at filling factor $\nu = 1/2$, the persistent current amplitude is independent of the size of the cluster. This statement is true only at $\nu = 1/2$ and it is in contradiction to a naive notion that the persistent current in a metallic phase is always mesoscopically small. Chapter 3 describes the numerical technique and gives some general results. In Chapter 4 the results of 2D computations are presented. A simple picture of the transition is formulated based on the comparison of the numerical data for different types of interaction potential. An empirical criterion is proposed, which allows estimation of the critical hopping amplitude J_c. In Chapter 5 we apply our empirical criterion to the 1D system with the Coulomb interaction and with the nearest- and the next-nearest interactions and show that it works very well even in a nontrivial situation. The criterion predicts existence of the metallic phase at any strong interaction for the model with next-nearest interaction. This phase is found and studied numerically.

CHAPTER 2

PERSISTENT CURRENT OF FREE FERMIONS

2.1 Introduction

Persistent current (PC) in mesoscopic structures[15, 17] has been extensively studied during the last decade both experimentally[18, 19, 20] and theoretically. The theoretical investigations concentrated on the role of different degrees of disorder[21, 22] and on the role of the interaction between electrons[23, 24].

The PC is the reaction of a system to an applied flux Φ, or, equivalently, it can be described as a change of the energy of the system due to twisted boundary conditions. In a 2D system that forms a cylinder the twisted conditions mean that the wave function of a system acquires a factor $\exp(i2\pi\Phi/\phi_0)$ with a circulation of one electron around the axis of the cylinder. Here $\phi_0 = hc/e$ is the flux quanta.

The flux Φ is related to the tangential component A of the vector potential $\Phi = 2\pi RA$, where R is the radius of the cylinder. For a system with Galilean invariance the following simple statement is correct. The energy of a state with a given value of tangential component P of the total momentum depends on A as

$$E(P, A) = E_0 - \frac{1}{2M}\left(P - \frac{Ne}{c}A\right)^2, \tag{2.1}$$

where N is the number of electrons and $M = Nm$ is their total mass, m being the mass of one electron. The 2D current density j for a state with fixed P is

$$j_P = -\frac{c}{S}\left(\frac{\partial E}{\partial A}\right)_P = -\frac{ne^2}{mc}A + \frac{eP}{mS}, \tag{2.2}$$

where S is the area of the cylinder surface and $n = N/S$. At $P = 0$ Eq. (2.2) reminds the London equation for a superconducting current. In this case n should be the superfluid density.

A general derivation of Eq. (2.2), given above, is misleading because PC should be defined as a current in the ground state rather than in a state with fixed P. In 2D or 3D

systems of free electrons the derivative of the energy with respect to A cannot be taken in such a simple way because the intervals of Φ, where branches of a spectrum with different P change each other in the ground state, tend to zero with increasing system size.

For electrons in a periodic potential the situation is typically similar. The derivative of energy with respect to the flux is large for a given branch. However, different branches replace each other in the ground state at such small intervals of Φ that the derivative taken at a given total quasimomentum P does not reflect properties of the ground state. Scalapino et al.[16] considered a tight binding model on a 2D square lattice. Their computations show that at filling factor $\nu = 1/4$ the first level crossing occurs at $\Phi \sim 1/L$, where L is the size of the system. Their general conclusion is that the superfluid density, as found from the relation between j and A, is zero for free electrons in the tight binding model. We show in this paper that this is not always the case.

Namely, we consider a 2D system of free electrons on a square lattice in a tight binding approximation at filling factor $\nu = 1/2$. The shape of the system is assumed to be a rectangle with arbitrary aspect ratio. We demonstrate below that at $T = 0$ the 2D PC density does not depend on the size of the system and has the form:

$$j = -\frac{4}{\pi^2}\,\frac{ne^2}{mc}(A - A_0). \tag{2.3}$$

Here $m = \hbar^2/2ta^2$ is the electron mass, t being the nearest-neighbor hopping energy. The 2D density is determined as $n = 1/2a^2$, where a is the lattice constant. For simplicity, we consider a system of spinless fermions. The generalization to the case of noninteracting fermions with spin is straightforward.

The constant A_0 shows that the minimum of energy occurs at nonzero flux. In contrast to Eq. (2.2), Eq. (2.3) describes PC in the ground state of the system which is a periodic function of Φ with period ϕ_0/q. Eq. (2.3) is valid within the interval $0 < \Phi < \phi_0/q$, or $0 < A < \phi_0/2\pi Rq$, and is to be repeated periodically for other values of flux. Here q is an integer that depends on the aspect ratio of the cylinder and on the type of the boundary conditions imposed in the direction of the cylinder axis. The first term is shown to be independent on the aspect ratio.

We found PC to have an order of magnitude of the London current. Note that this result gives substantially larger PC than is prescribed in the ballistic regime by the so-called M-channel approximation (see Ref.[25] and references therein). Namely, our

exact solution gives PC larger by a factor of $\sqrt{L}$ for the $L \times L$ square. This discrepancy is due to the fact that in the case of a flat Fermi surface all transverse channels are coherent.

Considering the 3D system constructed of a large number of coaxial closely packed 2D cylinders we show that it mimics the Meissner effect and the quantization of flux trapped in the opening.

These properties appear since the Fermi surface at $\nu = 1/2$ is flat and no branch crossings occur in large intervals of Φ. Say, for a square array no branch crossing occurs in the whole interval $0 < \Phi < \phi_0$, which means that $q = 1$.

In fact, we are discussing a mesoscopic effect. The expression Eq. (2.3) is valid only at mesoscopically small temperatures, and the ideal diamagnetism occurs for mesoscopically small values of magnetic field:

$$T < T_c \sim \frac{a}{R_{ef}} t, \tag{2.4}$$

$$H < H_c \sim \frac{a}{R_{ef}} \sqrt{\frac{t}{a^2 b}}, \tag{2.5}$$

where b is the spacing between neighboring coaxial cylinders. The effective size R_{ef} is given by

$$R_{ef} = sD = q2\pi R = \sqrt{sq2\pi RD}, \tag{2.6}$$

where D is the length of the cylinders and s and q are integers determined by the aspect ratio $2\pi R/D$ (see below). Thus, this system can be classified as a "mesoscopic superconductor."

Note that the average distance between energy levels in a 2D system is proportional to $1/R^2$. The $1/R$ behavior in the above equations is also a result of the flat Fermi surface at $\nu = 1/2$. As is seen from the calculations, all relevant interlevel distances are of the order of $(a/R)t$, rather than $(a/R)^2 t$.

Since both T_c and H_c vanish at large R, there are no real critical phenomena in this model system.

2.2 Calculation of PC at zero temperature

Consider a rectangle of $L_x \times L_y$ lattice sites with periodic boundary conditions twisted in both directions by $2\pi\Phi_x/\phi_0$ and $2\pi\Phi_y/\phi_0$. This corresponds to a toroidal geometry

where Φ_x is the flux through the crossection of the torus and Φ_y is the flux through the opening.

The single-electron energies have the form

$$\epsilon(n_x, n_y, \phi_x, \phi_y) = -2J \left\{ \cos\left[\frac{2\pi}{L_x}(n_x - \phi_x)\right] + \cos\left[\frac{2\pi}{L_y}(n_y - \phi_y)\right] \right\}, \qquad (2.7)$$

where we introduce dimensionless $\phi_{x,y} = \Phi_{x,y}/\phi_0$ to simplify the notation. The values of integer quantum numbers n_x and n_y are restricted to the rectangle $|n_{x,y}| \leq L_{x,y}/2$ (first Brillouin zone). To find the energy of the ground state one has to sum $\epsilon(n_x, n_y)$ over the values $\{(n_x, n_y)\}$ inside the Fermi surface.

In principle, the calculation of PC can be performed either at a constant number of particles N or at a constant value of chemical potential μ. Generally speaking, these two definitions are not equivalent. It is important to note that such a problem does not exist at $\nu = 1/2$ at even numbers of L_x, L_y at least. As one can see from Eq. (2.7), every single-electron energy changes sign under the transformation $n_x, n_y \to n_x + L_x/2, n_y + L_y/2$. It follows that at $\nu = 1/2$ due to the electron-hole symmetry the chemical potential μ is zero at any value of flux and at any temperature. Thus, if the flux changes at $\mu = 0$, the number of particles in the ground state of the system does not change and if the flux changes at a given number of particles such that $\nu = 1/2$, the chemical potential does not change.

Let us define the Fermi "surface" (FS) in 2D n_x, n_y space by the equation

$$\epsilon(n_x, n_y, \phi_x, \phi_y) = 0, \qquad (2.8)$$

considering n_x, n_y as continuous variables. It is easy to see that the FS forms a rhomb at any value of flux. Change in the flux produces a shift of the FS as a whole without changing its shape.

First, let us consider for simplicity a square sample, $L_x = L_y$. The FS forms a square as shown in Fig. 2.1a. At $\phi_{x,y} = 0$ some of the allowed single-electron states lie exactly at the sides of this square. All the states inside the square and 1/2 of the states at the sides of the square are occupied. All the states at the sides have the same energy so the occupation numbers of these states are not defined, whereas the many-electron ground state is degenerate.

The degeneracy is lifted at infinitazimally small values of ϕ. Suppose that $\phi_y = 0$ and $\phi_x > 0$. Then FS is shifted to the right (see Fig. 2.1a). All occupation numbers become

defined. Namely, the states at the right side of initial square get occupied and those at the left side become empty. Note that the occupation numbers of as many as $2L$ states change when ϕ_x crosses zero.

It is easy to see that the occupation numbers are constant throughout the interval $0 < \phi_x < 1$. The total energy decreases with ϕ_x and then increases again. At $\phi_x = 1$ all electrons jump one step to the right and the Fermi surface restores its original position with respect to the lattice of integer numbers (n_x, n_y). The total energy thus returns to the same value as at $\phi_x = 0$.

It follows that the total quasimomentum of electron system in the ground state does not change through all this interval and no branch crossing occurs. Then the sum over the occupied states can be easily evaluated:

$$E(\phi_x, \phi_y) = \sum_{n_y=1}^{L/2-1} \sum_{n_x=-L/2+n_y+1}^{L/2-n_y} [\epsilon(n_x, n_y) + \epsilon(n_x, -n_y)] + \sum_{n_x=-L/2+1}^{L/2} \epsilon(n_x, 0) \quad (2.9)$$

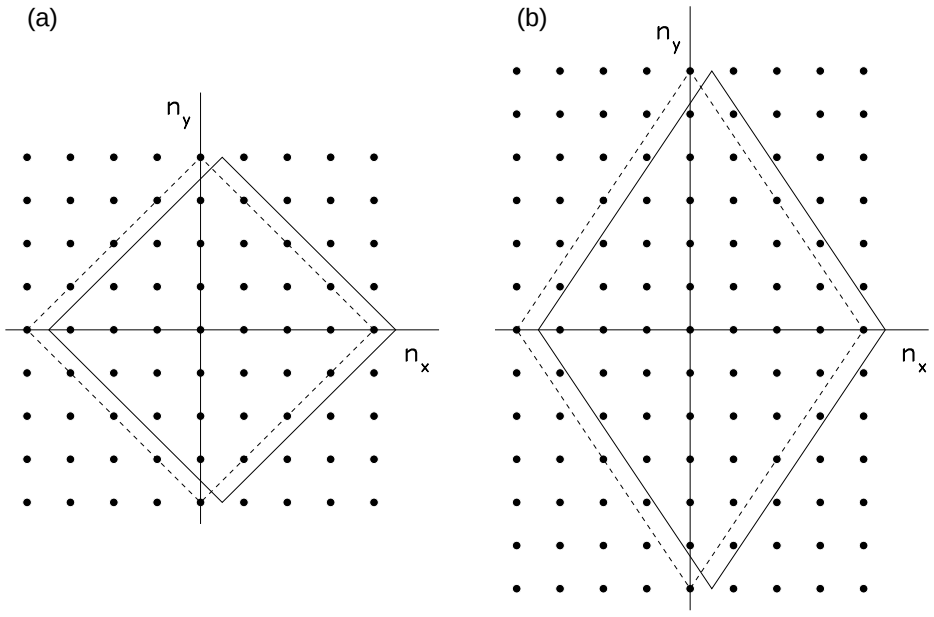

Figure 2.1. The Fermi surface at $\nu = 1/2$. The points represent allowed integer values of n_x and n_y inside the first Brillouin zone. The dashed lines show the Fermi surface at zero flux. The solid lines are the Fermi surface shifted by flux. The aspect ratio $L_x/L_y = 1$ (a) and $L_x/L_y = 2/3$ (b).

$$= \quad 8t\ Re\frac{e^{2\pi i/L}}{(e^{2\pi i/L}-1)^2}\left[\left(1+e^{2\pi i/L}\right)e^{-i2\pi\phi_x/L}+2e^{-i2\pi\phi_y/L}\right]$$

This expression is exact in the region $0 < \phi_x \pm \phi_y < 1$. In the limit of large L, the ϕ-dependent part of the energy, $\delta E(\phi_x, \phi_y) = E(\phi_x, \phi_y) - E(0,0)$, can be written in the form:

$$\delta E(\phi_x, \phi_y) = 8t\left[\phi_y^2 - \phi_x(1-\phi_x)\right]. \tag{2.10}$$

Repeating Eq. (2.10) periodically one gets the expression valid in the whole plane (ϕ_x, ϕ_y):

$$\delta E(\phi_x, \phi_y) = 4t\left[\left(\{\phi_+\}-\frac{1}{2}\right)^2+\left(\{\phi_-\}-\frac{1}{2}\right)^2-\frac{1}{2}\right], \tag{2.11}$$

where $\phi_\pm = \phi_x \pm \phi_y$, and $\{...\}$ denotes the fractional part of the number, defined as a difference between the number and the largest integer less than it.

Fig. 2.2 shows the energy $\delta E(\phi_x, \phi_y)$ as given by Eq. (2.11). The positions of energy minima form a square lattice shifted from the origin:

$$(\phi_x, \phi_y) = \left(\frac{1+i+j}{2}, \frac{i-j}{2}\right), \tag{2.12}$$

with arbitrary integer i and j.

The point $\phi_x = \phi_y = 0$ corresponds to a maximum of energy, in the same way as in the 1D case with an even number of electrons. At this point the derivatives $d\delta E/d\phi_{x,y}$

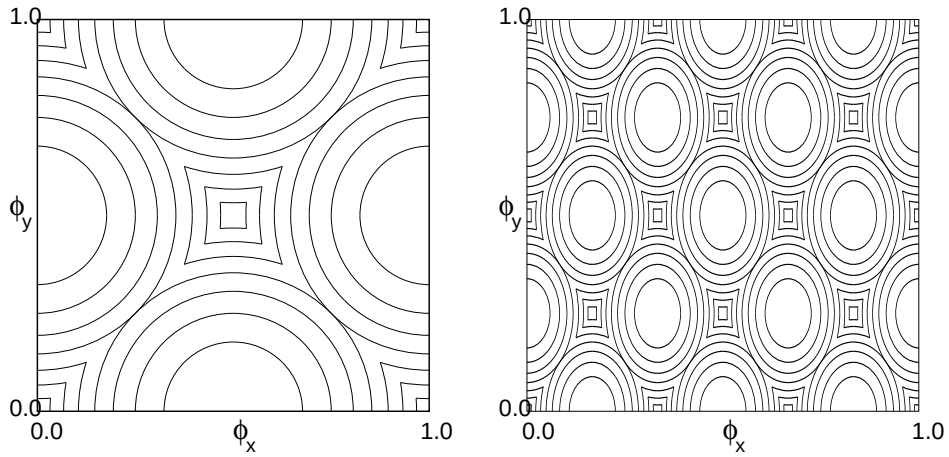

Figure 2.2. Lines of constant $\delta E(\phi_x, \phi_y)$ as given by Eq. (2.16) for square sample $s = q = 1$ (a), and for rectangle with $s = 2$ and $q = 3$ (b). Note the difference in periodicities.

are discontinuous. Such behavior appears as the result of lifting the degeneracy of the states at the Fermi surface.

The PC at $T = 0$ can be found as the derivative of the total energy with respect to flux:

$$\begin{aligned} I_{x,y} &= -c\frac{\partial E}{\partial \Phi_{x,y}} = -\frac{c}{\phi_0}\left(\frac{\partial E}{\partial \phi_+} \pm \frac{\partial E}{\partial \phi_-}\right) \\ &= -8\frac{ct}{\phi_0}\left[\left(\{\phi_+\} - \frac{1}{2}\right) \pm \left(\{\phi_-\} - \frac{1}{2}\right)\right] \end{aligned} \tag{2.13}$$

The magnitude of $\delta E(\phi_x, \phi_y)$ and $I_{x,y}(\phi_x, \phi_y)$ as given by Eqs. (2.11), (2.13) is independent of the size L of the square. Such a large magnitude results from the fact that in the region with no branch crossings (or, with no electron changing its state) all electrons together contribute to the current.

It may seem that the aspect ratio L_x/L_y equal to 1 is crucial for the effect. In the next section we calculate PC at finite temperature for arbitrary aspect ratio $L_x = sK$, $L_y = qK$ with mutually-prime integers s and q. We assume macroscopic limit $K \to \infty$. It is useful to generalize $\phi_\pm$ for a rectangular sample as

$$\phi_\pm = q\phi_x \pm s\phi_y. \tag{2.14}$$

In the limit $T = 0$ we find

$$\begin{aligned} I_x &= -\frac{8}{sq}\frac{ct}{\phi_0/q}\left[\left(\{\phi_+\} - \frac{1}{2}\right) + \left(\{\phi_-\} - \frac{1}{2}\right)\right] \\ I_y &= -\frac{8}{sq}\frac{ct}{\phi_0/s}\left[\left(\{\phi_+\} - \frac{1}{2}\right) - \left(\{\phi_-\} - \frac{1}{2}\right)\right] \end{aligned} \tag{2.15}$$

The flux-dependent part of the energy can be restored from Eq. (2.15):

$$\delta E(\phi_x, \phi_y) = \frac{4t}{sq}\left[\left(\{\phi_+\} - \frac{1}{2}\right)^2 + \left(\{\phi_-\} - \frac{1}{2}\right)^2 - \frac{1}{2}\right], \tag{2.16}$$

This result is a generalization of Eq. (2.11) to an arbitrary aspect ratio s/q of the rectangular sample.

As follows from Eqs. (2.15), (2.16), the energy and current as functions of flux depend on the aspect ratio. However, they do not depend on the system size, if the aspect ratio is kept constant.

The result given by Eqs. (2.15) and (2.16) can be understood from Fig. 2.1b, which is drawn for the case $L_x/L_y = 2/3$. Contrary to Fig. 2.1a, there are now points (n_x, n_y) closer to the Fermi surface than one lattice spacing. However, there is still a regularity in their positions. Namely, as the Fermi surface shifts with flux, the points enter the Fermi sea in groups. Consider, for example, the same case as above: $\phi_y = 0$ and $\phi_x > 0$. As seen in Fig. 2.1b, the branch crossings occur only at $\phi_x = 2\pi/3$, $4\pi/3$, and 2π. In terms of $\phi_\pm$ this corresponds to integer $\phi_\pm = 3\phi_x = 1$, 2, and 3. These values of flux are determined by s and q and do not change with the size of the system. The number of points in each group, in turn, is proportional to the size of the system, so the corresponding contribution to the current is large.

At $\Phi_y = 0$ Eq. (2.15) gives

$$I_x = -\frac{16}{sq}\frac{ct}{\phi_0/q}\left(\left\{\frac{\Phi_x}{\phi_0/q}\right\} - \frac{1}{2}\right). \tag{2.17}$$

Up to now we have been discussing the torus geometry. To come to a cylinder geometry one has to formulate the boundary conditions in the direction of the cylinder axis, chosen as y. In what follows we assume periodic boundary conditions in this direction with $\Phi_y = 0$. This leads to Eq. (2.17) for a total current through the cylinder. As another option we may impose the condition that the wave function is zero at the edges of the cylinder. It can be shown that in this case the second term in Eq. (2.17) changes whereas the first term remains intact.

Note that both energy and current are periodic functions of flux with period ϕ_0/q rather than ϕ_0.

Taking into account that the current density $j_x = I_x/(aL_y)$ and that the vector potential $A_x = \Phi_x/(aL_x)$ one obtains Eq. (2.3) with the first term independent of s and q.

2.3 PC at finite temperature

We start with the equation

$$I_x = -\frac{c}{\phi_0}\sum_{n_x=0}^{sK-1}\sum_{n_y=0}^{qK-1}\frac{\partial\epsilon(n_x,n_y)}{\partial\phi_x}\frac{1}{1+\exp(\epsilon(n_x,n_y)/T)}. \tag{2.18}$$

It is convenient to rewrite the single electron energy in the form

$$\epsilon(n_x, n_y) = -4t \cos\left(\frac{\pi}{sqK}(n_+ - \phi_+)\right) \cos\left(\frac{\pi}{sqK}(n_- - \phi_-)\right), \tag{2.19}$$

where $n_\pm = qn_x \pm sn_y$ and $\phi_\pm$ are given by Eq. (2.14). Using $\partial/\partial\phi_x = q(\partial/\partial\phi_+ + \partial/\partial\phi_-)$ we find that the current has two terms,

$$I_x = \frac{1}{s}(I_+ + I_-), \tag{2.20}$$

where

$$I_\pm = -sq\frac{c}{\phi_0}\sum_{n_x=0}^{sK-1}\sum_{n_y=0}^{qK-1}\frac{\partial\epsilon(n_x, n_y)}{\partial\phi_\pm}\frac{1}{1+\exp(\epsilon(n_x, n_y)/T)} \tag{2.21}$$

The idea of our calculation is to transform Eq. (2.21) in such a way that the internal sum gives PC of 1D problem with effective temperature and effective flux. For this purpose we use the identity:

$$\sum_{n_x=0}^{sK-1}\sum_{n_y=0}^{qK-1} f(n_x, n_y) = \sum_{m=0}^{sK-1}\sum_{d=0}^{q-1}\sum_{k=0}^{K-1} f(m + d + sk, d + qk). \tag{2.22}$$

This identity is valid for any function $f(n_x, n_y)$ periodic in n_x and n_y with periods sK and qK respectively. Then I_+ can be written in the form

$$I_+ = -\frac{4\pi ct}{K\phi_0}\sum_{m=0}^{sK-1}\sum_{d=0}^{q-1}\sum_{k=0}^{K-1}\frac{\sin\left(\frac{\pi}{sqK}(n_+ - \phi_+)\right)\cos\left(\frac{\pi}{sqK}(n_- - \phi_-)\right)}{1+\exp\left[-\frac{4t}{T}\cos\left(\frac{\pi}{sqK}(n_+ - \phi_+)\right)\cos\left(\frac{\pi}{sqK}(n_- - \phi_-)\right)\right]}. \tag{2.23}$$

A similar expression can be written for I_-. Note that $n_- = qm + (q-s)d$ does not depend on k, while $n_+ = (qm + qd + sd) + 2sqk$ does depend on k. Therefore, the current I_+ can be written as

$$I_+ = \sum_{m=0}^{sK-1}\sum_{d=0}^{q-1}\mathcal{I}_+(m, d), \tag{2.24}$$

where $\mathcal{I}_+(m, d)$ denote the internal sum over k,

$$\mathcal{I}_+(m, d) = -\frac{4\pi ct}{K\phi_0}\frac{2T}{\widetilde{T}}\sum_{k=0}^{K-1}\frac{\sin\left(\frac{2\pi}{K}(k - \widetilde{\phi}_+)\right)}{1+\exp\left[-\frac{2t}{\widetilde{T}}\cos\left(\frac{2\pi}{K}(k - \widetilde{\phi}_+)\right)\right]}. \tag{2.25}$$

The sum in Eq. (2.25) describes the PC in 1D system with effective temperature and effective flux given by

$$\begin{aligned} \widetilde{T}(m,d) &= \frac{T}{2\cos\left(\frac{\pi}{sqK}(qm+(q-s)d-\phi_-)\right)} \\ \widetilde{\phi}_+(m,d) &= \frac{\phi_+ - qm - qd - sd}{2sq} \end{aligned} \tag{2.26}$$

Using the Poisson summation formula (see Ref. [29]), one obtains

$$\mathcal{I}_+(m,d) = \frac{8\pi cT}{\phi_0}\sum_{l=1}^{\infty}\frac{\cos(l\pi K/2)}{\sinh(l\pi\widetilde{T}K/2t)}\sin(2\pi l\widetilde{\phi}_+) \tag{2.27}$$

Performing the summation over m and d in Eq. (2.24) we note that $\widetilde{T}$ is a smooth function of m/K and d/K. However, $\sin(2\pi l\widetilde{\phi}_+)$ has an oscillatory behavior for some l, so that the contribution of the corresponding harmonics vanishes in the limit $K\to\infty$. The oscillatory behavior is absent if l is an integer multiple of $2sq$. For these l, the sum over m can be transformed into integral via $p=(\pi/sK)m$, while the sum over d simply gives a factor q. Thus, one obtains

$$I_\pm = \sum_{l=1}^{\infty} A_l \sin(2\pi l\phi_\pm), \tag{2.28}$$

where

$$A_l = sqKT\frac{2c}{\phi_0}\int_0^\pi \frac{dp}{\sinh(l\pi sqKT/2t\sin p)} \tag{2.29}$$

For the PC in x-direction one has from Eq. (2.20)

$$I_x = \frac{1}{s}\sum_{l=1}^{\infty} A_l\left[\sin(2\pi l\phi_+)+\sin(2\pi l\phi_-)\right]. \tag{2.30}$$

Similar calculation gives

$$I_y = \frac{1}{q}\sum_{l=1}^{\infty} A_l\left[\sin(2\pi l\phi_+)-\sin(2\pi l\phi_-)\right]. \tag{2.31}$$

Eqs. (2.29) and (2.30) give the Fourier series expansion of PC at any temperature. Expansion of A_l at small KT/t yields

$$A_l \approx \frac{8t}{\phi_0}\frac{1}{l\pi} \tag{2.32}$$

In this case Eqs. (2.30), (2.31), and (2.32) give the Fourier series expansion of the zero-temperature result Eq. (2.15).

In the opposite limit, $KT/t \gg 1$, the amplitudes of the harmonics decay as

$$A_l \approx \frac{8c}{\phi_0\sqrt{l}}\sqrt{sqKTt}\exp\left(-\frac{l\pi sqKT}{2t}\right), \tag{2.33}$$

so that PC is dominated by its lowest harmonic. When $\Phi_y = 0$ one has

$$I_x \approx \frac{1}{sq}\frac{16c}{\phi_0/q}\left(\frac{R_{ef}Tt}{a}\right)^{1/2}\exp\left(-\frac{\pi R_{ef}T}{2at}\right)\sin\left(\frac{\Phi_x}{\phi_0/q}\right). \tag{2.34}$$

2.4 Low temperature magnetic properties

In this section we study magnetic properties of a quasi-3D system constructed of a macroscopic number of closely packed coaxial cylinders assuming that the temperature is very low. Then the connection between flux and current for each cylinder is given by Eq. (2.17). For the sake of simplicity we assume that the cylinders are long, such that the circumference of the internal cylinder $2\pi R = aL_x$ is much larger than $D = aL_y$. The distance between the internal and external cylinders is supposed to be much less than R. We assume further that all the cylinders have the same ratio $L_x/L_y = s/q$. One can imagine a small change either in L_x and L_y of adjacent cylinders or in their lattice constant.

The second term in Eq. (2.17) appears since zero flux does not correspond to the minimum of energy. It may lead to an appearance of a spontaneous flux in this system. This idea has been put forward by Wohlleben et al. and Szopa and Zipper, Ref. [26], and then studied in details in Ref. [27]. These authors considered a cylinder constructed from isolated 1D rings. Loss and Martin[28] argued that in a single 1D ring no symmetry breaking can occur, but their arguments are restricted to the 1D case.

In this paper we concentrate on the first term in Eq. (2.17). It is an analog of the London current in superconductors and it creates a strong diamagnetism in a quasi-3D system described above. Suppose that an external magnetic field H_{ext} is applied to the system and that there is a solenoid creating flux Φ_{ext} inside the internal cylinder.

Let Φ_k be the total flux inside cylinder k, where $k = 1$ for the internal cylinder and $k = N$ for the external one. The flux obeys the equation

$$\Phi_k - \Phi_{k-1} = 2\pi Rb\left(H_{ext} + \frac{4\pi}{cD}\sum_{i=k}^{N} I(\Phi_i)\right). \tag{2.35}$$

Here b is the distance between adjacent cylinders which we assume to be of the order of the lattice constant a. Since the thickness $d = Nb$ is supposed to be much less than R we

have neglected the fact that the radii of cylinders are slightly different. The right hand side of Eq. (2.35) describes the flux through the area between the k-th and $(k-1)$-th cylinders created by the external field and outer cylinders.

The following condition should be added to this finite difference equation:

$$\Phi_1 - \Phi_{ext} = \pi R^2 \left(H_{ext} + \frac{4\pi}{cD} \sum_{i=1}^{N} I(\Phi_i) \right). \tag{2.36}$$

If Φ_k is a smooth function of k one can transform Eq. (2.35) into differential equation

$$\frac{d^2\Phi}{dr^2} = \frac{\phi_0/q}{\lambda^2} \left(\left\{ \frac{\Phi}{\phi_0/q} \right\} - \frac{1}{2} \right). \tag{2.37}$$

Here λ is the analog of the London penetration depth

$$\lambda^{-2} = \frac{4\pi}{b} \frac{16t}{\phi_0^2} = \frac{16e^2 n_3}{\pi m c^2}, \tag{2.38}$$

where $n_3 = 1/2ba^2$ is the 3D electron density.

Eq. (2.36) transforms into the boundary condition at $r = R$:

$$\Phi(R) - \Phi_{ext} = \frac{R}{2} \left. \frac{d\Phi}{dr} \right|_{r=R}. \tag{2.39}$$

The second boundary condition reads

$$\left. \frac{d\Phi}{dr} \right|_{r=R+d} = 2\pi R H_{ext}. \tag{2.40}$$

One can use THE differential equation if $\lambda \gg b$.

Eq. (2.37) can also be obtained by minimizing total energy with respect to flux. The total energy consists of two parts. First is the energy of magnetic field in the space between cylinders. The magnetic field can be expressed through $d\Phi/dr$ using Eq. (2.35) as

$$\frac{d\Phi}{dr} = 2\pi R H(r). \tag{2.41}$$

The second part is the internal energy of 2D electron gas. This energy per cylinder is given by Eq. (2.16) at $\phi_y = 0$. Thus, one gets for the total energy

$$E_{total} = \frac{1}{8\pi} \frac{D}{2\pi R} \int \left(\frac{d\Phi}{dr} \right)^2 dr + \int \delta E(\Phi) \frac{dr}{b}. \tag{2.42}$$

Minimizing this expression with respect to $\Phi(r)$ and taking into account that $d\delta E/d\Phi = (-1/c)I(\Phi)$, where $I(\Phi)$ is given by Eq. (2.17), one obtains Eq. (2.37).

The Eq. (2.37) is nonlinear since it contains the fractional part $\{\Phi/(\phi_0/q)\}$ which makes the right-hand side periodic. However, it becomes linear if the total drop of the flux inside the system is smaller than ϕ_0/q. If $H_{ext} = 0$ the solution of the linearized equation with boundary conditions (2.39), (2.40) in the case $R \gg d \gg \lambda$ is

$$\Phi(r) = \Phi_n + (\Phi_{ext} - \Phi_n)\frac{2\lambda}{R}\exp\left(-\frac{r-R}{\lambda}\right). \tag{2.43}$$

Here

$$\Phi_n = \frac{\phi_0}{q}\left(n - \frac{1}{2}\right). \tag{2.44}$$

One can see that the flux inside the cylinder with $d \gg \lambda$ may take only quantized values Φ_n with arbitrary integer n. Note that there is no zero flux among the allowed values of the frozen flux Φ_n. This is because zero flux does not correspond to a minimum of the total energy at zero temperature. The solution Eq. (2.43) is obtained in the linear approximation and it is valid if $(\Phi_{ext} - \Phi_n)2\lambda/R < \phi_0/q$. The physics of this result is that the inner cylinders carry a current that creates a favorable flux for the rest of the system.

If the system is in an external magnetic field H_{ext}, the solution is

$$\Phi(r) = \Phi_n + 2\pi R\lambda H_{ext}\exp\left(-\frac{R+d-r}{\lambda}\right). \tag{2.45}$$

or in terms of magnetic field defined by Eq. (2.41)

$$H(r) = H_{ext}\exp\left(-\frac{R+d-r}{\lambda}\right) \tag{2.46}$$

In this case the cylinders near external surface carry current that screens magnetic field inside the system and adjusts the total flux to Φ_n. The solution is valid if $2\pi R\lambda H_{ext} < \phi_0/q$. This condition is equivalent to Eq. (2.5). It has a simple interpretation. The loss in the total energy due to the ideal Meissner effect is of the order of $H_{ext}^2 RDb$ per cylinder. The gain in the energy of a cylinder due to the adjusted flux is of the order of t/sq (see Eq. (2.16)). At large field the loss becomes larger than the gain and the field penetrates into the system. This is the origin of a "mesoscopic" critical field. Note that the relation $H_c^2 RDb \sim t/sq$ is also equivalent to Eq. (2.5).

It follows from the results of the previous section that zero-temperature approximation is good if $sqKT/t = T\sqrt{sq2\pi RD}/at \ll 1$. This is the same condition as Eq. (2.4). At

larger temperatures the penetration depth λ increases as $\exp(\pi T R_{ef}/4at)$ and eventually reaches the thickness d of the cylinder, gradually destroying strong diamagnetism.

2.5 Conclusions

Finally we have presented a model that mimics in a mesoscopic scale some properties of superconductors, such as Meissner effect and quantization of flux, though the physics of the model does not involve any electron pairing. The flux quanta in the model is ϕ_0/q where q is determined by the aspect ratio of the system.

Since the range of temperature and magnetic field for these phenomena shrink to zero in a macroscopic system, one should not expect any phase transitions. However, for a mesoscopic system this range is not necessarily small. Let us assume a hypotetic 3D layered system with very weak interaction between layers and flat 2D Fermi surface. Then it follows from Eqs. (2.4), (2.5) that the temperature range is up to 12K and the range of H_{ext} is up to 240 gauss for a system with $R_{ef} = 3 \times 10^{-5}$cm, $a = b = 3 \times 10^{-8}$cm, and $t = 1$eV. In a system with disorder the obvious condition for these phenomena is that the elastic mean free path is smaller than the size R_{ef}.

Our model ignores electron-electron interaction. We hope that it is not important at large t. Our modeling of small interacting systems up to 16 electrons shows the same value of the PC at t immediately above the Wigner crystal quantum melting point (see Chapter 4).

CHAPTER 3

COMPUTATIONAL APPROACH AND GENERAL REMARKS

In the 2D case we consider Hamiltonian Eq. 1.1 with Coulomb potential $V(r) = 1/r$ and strongly screened Coulomb potential $V(r) = \exp(-r/r_s)/r$. We study rectangular clusters $L_x \times L_y$ with the periodic and twisted boundary conditions for the wave function. The dimensionless vector potential $\phi = (\phi_x, \phi_y)$ can be introduced in the Hamiltonian Eq. 1.1 by subsitution of $a^\dagger_{\mathbf{r}+\mathbf{s}} a_{\mathbf{r}} \to a^\dagger_{\mathbf{r}+\mathbf{s}} a_{\mathbf{r}} \exp(i\phi\mathbf{s})$. This substitution is equivalent to the twist of the boundary conditions by the flux $\Phi_i = L_i\phi_i$, $i = x, y$. The total spectrum is periodic in Φ_x and Φ_y with the period 2π.

As a basis for computations we use many-electron wave functions at $J = 0$: $\Psi_\alpha = \prod_{i=1}^{N} a_i^\dagger |\mathrm{VAC}>$. The total size of the Hilbert space is C_M^N, where $M = L_x \times L_y$ is the area of a system. It is effectively reduced about M times when the quasimomentum is introduced as prescribed below.

3.1 Low-energy spectrum at $J = 0$

The basic functions Ψ_α can be visualized in pictures, which we call *icons*. Some lowest energy icons for $\nu = 1/2$ and cluster size 4×6 are shown in Fig. 3.1. The energy of each icon has been calculated as a Madelung sum, assuming that the icons are repeated periodically over the infinite plane with a compensating homogeneous background.

The icon with the lowest energy is a fragment of the crystal. In order to study quantum melting it is necessary to have the size of the cluster commensurate with the primitive vectors of the WC. In this case the periodic continuation does not destroy the crystalline order.

As we show below, the icon which corresponds to the lowest excited state plays crucial role in quantum melting. We denote the lowest excitation energy at $J = 0$ as Δ. It appears to be a general statement, that in a large enough cluster Δ corresponds to the energy of the lowest point defect in the WC (e.g., Fig. 3.1b). Indeed, the energy of

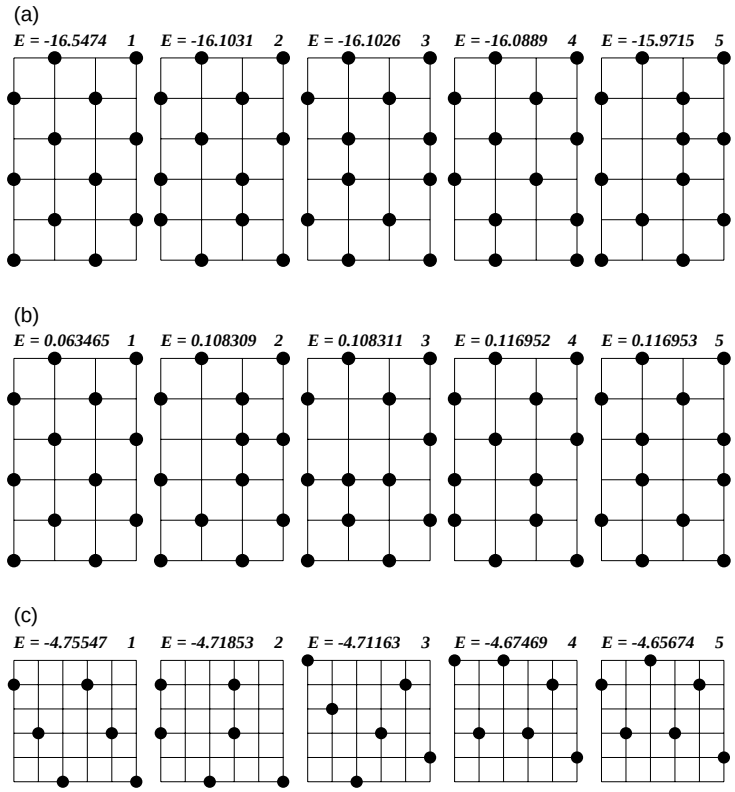

Figure 3.1. Icons with lowest energies for (a) $\nu = 1/2$, Coulomb interaction, (b) $\nu = 1/2$, short-range interaction, and (c) $\nu = 1/6$ Coulomb interaction.

such defect remains finite in large clusters, whereas the energy of any extended defect, like dislocation, increases linearly with the cluster size. Thus, at $J = 0$ the excitation spectrum of the system has a gap equal to the energy necessary to create a single point defect.

One can see from Fig. 1 that this is the case for short-range interaction, but not for the Coulomb interaction. For the Coulomb interaction at $\nu = 1/2$ the point-defect appears only as the fifth icon in the cluster 4×6. At $\nu = 1/6$ the icons shown in Fig. 3.1 do not contain a point defect at all.

We have studied thoroughly the low-energy spectrum for Coulomb interaction at $J = 0$. We analyzed square clusters with different sizes L and filling factors 1/2, 1/3, 1/4, and 1/6 using classical Monte-Carlo technique. The results are presented in Fig. 3.2. At $\nu = 1/3$ and 1/6 new low-energy types of dislocations appear with an increasing cluster size. These dislocations are restricted by the periodic conditions in smaller clusters. As a result, Δ decreases with size for small clusters. However, for large enough clusters new

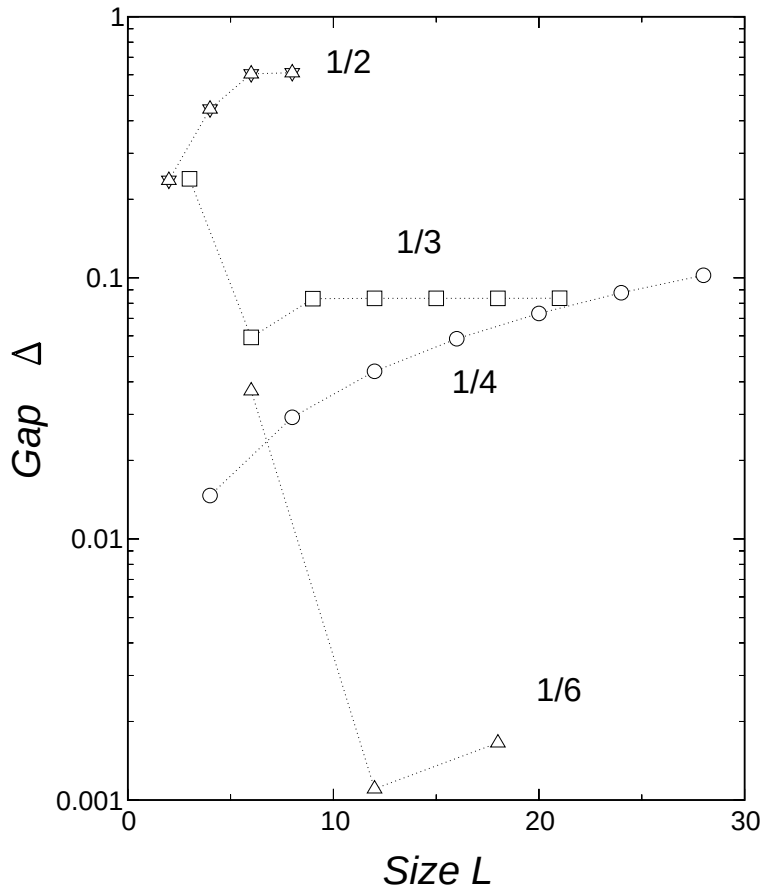

Figure 3.2. Size dependence of the lowest excitation energy at $J = 0$ for different filling factors. The saturation occurs at such size when the point defect becomes the lowest excitation.

dislocations do not appear so that Δ does not decrease. For $\nu = 1/2$ and $1/3$ the point defect becomes the lowest excited state starting with the square sizes 6×6 and 9×9 respectively. For $\nu = 1/4$ and $1/6$ we are unable to find this size. However, the increase of Δ with L assures that the point defect should finally become the lowest excited state starting with some large enough cluster.

3.2 Quasimomentum representation

The Hamiltonian Eq. 1.1 is translationally invariant. For each icon α there are m_α different icons that can be obtained from it by various translations. These icons are combined to get the wave function with total quasimomentum $\mathbf{P}$:

$$\Psi_{\alpha\mathbf{P}} = \frac{1}{\sqrt{m_\alpha}} \sum_{\mathbf{r}} \exp(i\mathbf{P}\mathbf{r}) T_{\mathbf{r}} \Psi_\alpha. \tag{3.1}$$

The summation is performed over m_α translations $T_{\mathbf{r}}$.

An important point is that the icons with periodic structures generate a smaller number of different functions $\Psi_{\alpha\mathbf{P}}$. The number of allowed $\mathbf{P}$ generated by each icon is equal to m_α. In particular, for the icon Ψ_0 of a WC with one electron per primitive cell, one has $m_0 = 1/\nu$. The allowed values of $\mathbf{P}$ can be determined from the conditions

$$(-1)^{Q_j} \exp(i\mathbf{P}\mathbf{l}_j) = 1. \tag{3.2}$$

Here $\mathbf{l}_j$ are the primitive vectors of the WC, and Q_j are the numbers of fermionic transmutations necessary for translations on these vectors. These conditions can be easily understood. If translation on a vector $\mathbf{l}_j$ is applied to Eq. (2), the right-hand side acquires a factor $(-1)^{Q_j}$, whereas for a function with given $\mathbf{P}$ this factor must be equal to $\exp(i\mathbf{P}\mathbf{l}_j)$. If Q_j are even for both $\mathbf{l}_j$, the allowed $\mathbf{P}$ form the reciprocal lattice of the WC. However, in the case when one or both of Q_j are odd, the lattice is shifted by π in the corresponding directions. In such case $\mathbf{P} = 0$ is forbidden. The complete set of m_α nontrivial values of $\mathbf{P}$ can be obtained by restricting $\mathbf{P}$ to the first Brillouin zone of the background lattice. One WC is represented by a number of icons obtained from each other by the point-group transformations of the background lattice. The total number of allowed values of $\mathbf{P}$ for the WC is the property of the WC and does not depend on the size and the shape of the cluster. On the contrary, an icon representing a point defect in a WC generates all vectors $\mathbf{P}$; their total number is M.

3.3 General remarks

The following results can be obtained directly using the perturbation theory with respect to J: (i) the ground state and the lowest excited states have a common large down shift that is proportional to J^2 and to the total number of particles N; (ii) the ground state splitting appears in the N-th order and it is proportional to J^N; (iii) the flux dependence of the ground state for the flux in x-direction appears in the L_x-th order and it is proportional to J^{L_x} in 2D case. In the 1D case the flux dependence appears in the N-th order and it is also proportional to J^N.

At small J there is a gap in the spectrum since a finite energy is required to create a point defect in the WC. The states originating from the WC icon do not belong to

the continuous spectrum since their number remains finite in a macroscopic system. The states originating from an icon with point defect in WC form a band.

One can imagine two different scenario of the transition. The simplest one is the first-order phase transition. It occurs if the branch originated from the point-defect icon crosses the ground state at $J = J_c$. This may happen because the energy of the bottom of the point-defect band is going down with increasing J and can overcome the Coulomb energy of the point defect existing at $J = 0$. The crossing is possible if the defect branch has $\mathbf{P}$ different from all vectors of the WC. Since the point defect may have all $\mathbf{P}$, the excitation spectrum of the large system will become continuous at $J > J_c$. Then the new state should be a normal metal.

In the second scenario the ground state eigenvector originated from the WC icon has an avoided crossing with defect states of the same $\mathbf{P}$. The ground state obtains a large admixture of the defect states, looses the structural long range order and becomes delocalized in terms of the persistent current. No level crossing occurs in this scenario, so the transition is not of the first-order transition. In all computational results that follow we observed the second scenario.

CHAPTER 4

RESULTS OF 2D COMPUTATIONS

Fig. 4.1a,b show the result of diagonalization for cluster 4×6 with 12 electrons for the long-range Coulomb interaction (a) and for the screened interaction (b) with $r_s = 0.25$. The last case can be considered as a short-range interaction. The total energy E is shown as a function of J. The ground state energy is taken as a reference point for E. Here and below, the unit of energy is the Coulomb interaction energy for nearest neighbors. At $J = 0$ the values of E coincide with the energies of the icons shown in Fig. 3.1. The zero-J gap Δ in the Coulomb case is almost exactly 10 times larger than in the short range case (see Fig. 3.1a,b).

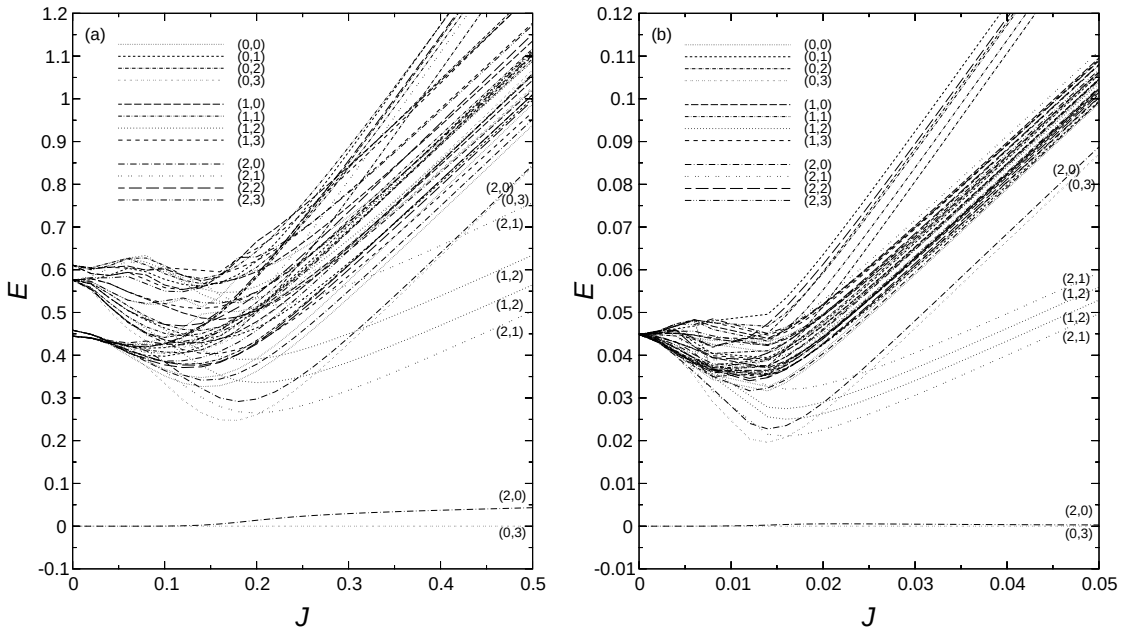

Figure 4.1. Low-energy part of the spectrum for the cluster 4×6 at $\nu = 1/2$ for (a) Coulomb interaction and (b) short-range interaction. The numbers (n_x, n_y) denote the components of quasimomentum $\mathbf{P} = (2\pi n_x/L_x, 2\pi n_y/L_y)$. The ground-state energy is taken as a reference point.

At large J the energy E is linear in J. Thus, we can conclude that with increasing J in this interval we go all the way from classical icons to free fermions. The ground state is almost degenerate at small J and it splits into two states with increasing J. As we have discussed above, this is a manifestation of the structural transition, which is the quantum melting of the WC. The quasimomenta of these two states are those generated by the WC icon, $\mathbf{P} = (0, \pi)$ and $(\pi, 0)$. In Fig. 4.1a,b they are denoted as (0,3) and (2,0), where (n_x, n_y) stands for quasimomentum with projections $P_x = 2\pi n_x/L_x$, $P_y = 2\pi n_y/L_y$. The other branches are the bands of defects.

Fig. 4.2a,b show flux sensitivity $\delta E = |E(\pi) - E(0)|$, computed for the states with lowest energy for both $\mathbf{P} = (0, 3)$ and (2,0), and the energy splitting between these states. In accordance with perturbation theory (see Sec. 3.3), the flux sensitivity at small J obeys the laws J^4 and J^6 for the direction of the vector potential along the short and long sides of the cluster respectively. The splitting is roughly proportional to J^{12}. At large J the flux sensitivity is linear in J and coincides with the free-fermion value. Note that for free

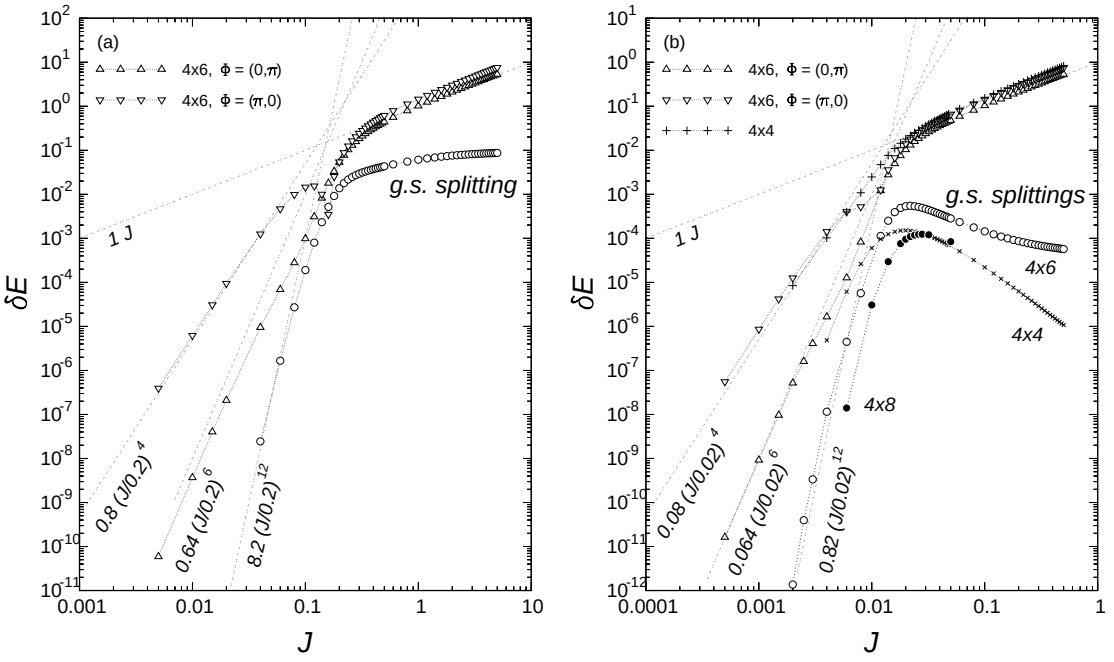

Figure 4.2. Flux sensitivity for different directions of vector potential and the ground-state splitting as a function of J for (a) Coulomb interaction and (b) short-range interaction. The value $J_c = 0.02$ is assumed. (b) A comparison of the results for different cluster sizes. No significant size dependence of J_c is observed.

fermions at $\nu = 1/2$ the flux sensitivity δE is size independent for large clusters, while it depends on the aspect ratio (see Chapter 3).

The data for δE and splitting imply that the structural transition and insulator-metal transition both occur between $J = 0.2$ and 0.3 for the Coulomb interaction, and between 0.02 and 0.03 for the short range interaction.

Comparison of Figs. 4.2a and 4.2b shows that the dependencies $\delta E(J)$ for the Coulomb and the short-range potential are almost indistinguishable if all the energy scales for one of them are adjusted 10 times. This factor is just the ratio of gaps Δ for these two cases. Thus, we come to a conclusion that the transition point is determined by the value of Δ and is almost independent of the type of interaction potential. The same applies to the general structure of the low-energy spectrum of the system in the transition region as can be seen from comparison of Figs. 4.1a and 4.1b.

Fig. 4.1 suggests the following mechanism of the transition. The width of the band of the lowest point defect in the WC increases with J such that its lowest edge comes close to the energy of the ground state[30]. Strong mixing between the crystalline and defect states occurs at this point. This simple picture implies that critical value of J is determined by the energy Δ of the lowest defect at $J = 0$. Now we can propose the empirical rule for J_c:

$$J_c = \beta\Delta \tag{4.1}$$

where β is some number. This number may depend on the type of the host lattice and filling factor. However, in all cases we have studied it is between 0.4 and 0.8. Say, in the case $\nu = 1/2$ we have $0.45 < \beta < 0.68$.

Fig. 4.3a,b shows the data for $\nu = 1/6$ and Coulomb interaction. Fig. 4.3a looks more complicated than Fig. 4.1a,b. The WC for this case is shown in the first icon in Fig. 3.1c. There exist four such WC that can be obtained from each other by point-symmetry operations. Each WC generates six different values of $\mathbf{P}$. Thus, at small J the ground state of the system is degenerate 24 times. Note that the multiplicity is large; however it still remains finite in the infinitely large system, where it is always equal to 24.

The primitive vectors of the WC can not be obtained from each other by any symmetry operation on the host lattice. This means that the WC phase belongs to a *reducible* representation of the symmetry group of the host lattice. Following Landau and Lifshitz[31], the symmetry reduction in the second-order phase transition should be such that the

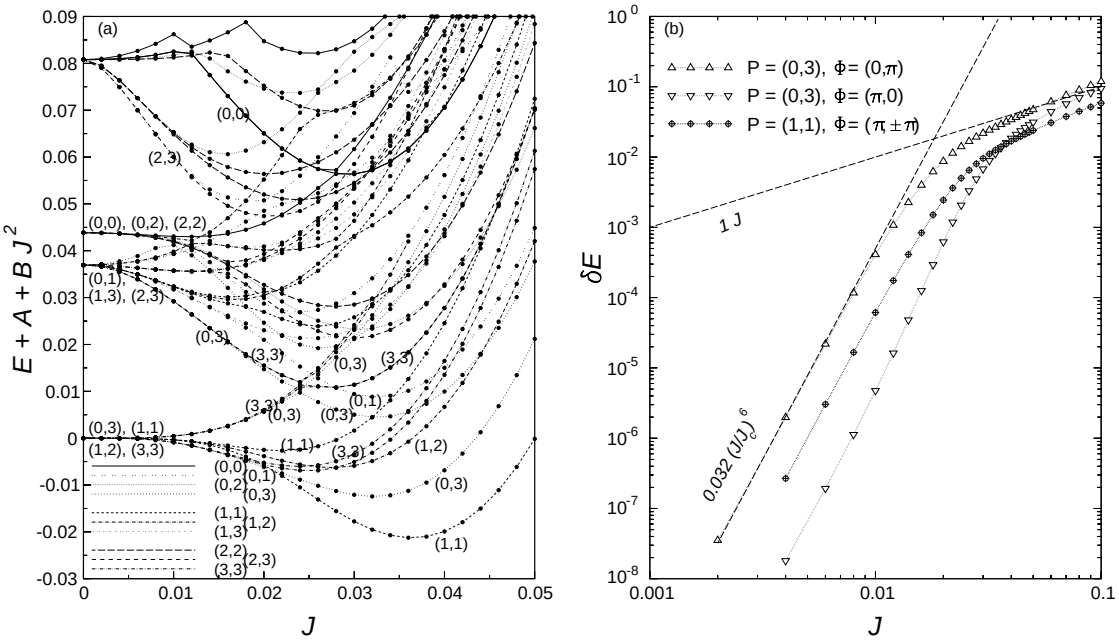

Figure 4.3. Computational results of the cluster 6×6(a) the low-energy part of the spectrum and (b) the flux sensitivity for different P and directions of flux for the cluster 6×6 at $\nu = 1/6$. The numbers (n_x, n_y) denote the components of quasimomentum $\mathbf{P} = (2\pi n_x/L_x, 2\pi n_y/L_y)$. The reference point is taken to be $A + BJ^2$, where A is the energy of the WC at $J = 0$, and $B = 177$ is the exact J^2 term as obtained from perturbation theory.

low-symmetry phase belongs to an irreducible representation of the symmetry group of the high-symmetry phase. We conclude that the single second order phase transition is forbidden in this case. However, it can occur as a series of the transitions, each reducing the symmetry one step further. In fact, Fig. 4.3a suggests that there are several transitions. We think that each splitting of the energy levels generated by the WC icon manifests a structural transition. The cluster size 6×6 is too small to distinguish the critical J for each of these transitions. We can only conclude that they all occur in the region $0.02 < J < 0.03$.

The metal insulator transition as seen in Fig. 4.3b also occurs in the same region of J. Taking into account the value $\Delta = 0.037$ for the cluster 6×6 we see that the parameter β in Eq. 4.1 is about $\beta \sim 0.5$–0.8. Note that for the pure Coulomb interaction the systems with $\nu = 1/2$ and $1/6$ differ in both Δ and J_c by a factor of 10, whereas the ratio Δ/J_c is almost the same.

The proposed mechanism of the transition can be illustrated by the dependence $E(\mathbf{P})$

at given J. Unfortunately, in 2D case the number of discreet values of $\mathbf{P}$ along any line in the first Brillouin zone is small even for the largest 2D system we study. However, such dependence is well pronounced in 1D. We discuss it in Sec. 4.1.

Now we study the size dependence of J_c at $\nu = 1/2$. As mentioned in Sec. 3.1, in the Coulomb case the gap Δ depends on the size of the cluster for small clusters. To avoid this difficulty we consider only the short-range potential, where such dependence is absent. To choose the size and a shape of the cluster we should keep in mind the condition of commensurability of the WC, mentioned in Sec. 3.1. Since we can study clusters up to 16 particles this condition restricts our options to clusters 4×4, 4×6, and 4×8 for $\nu = 1/2$.

The low-energy spectrum for the cluster 4×4 is shown in Fig. 4.3a. In this case the WC icon generates quasimomenta $\mathbf{P} = (0, 0)$ and (π, π). The flux sensitivity and the ground state splitting are shown in Fig. 4.3b. The transition point is again between $J = 0.02$ and 0.03. The ground state splitting for 4×8 is shown also in Fig. 4.2b. It is close to the splitting for 4×4 in the transition region. Thus, our data do not show any pronounced systematical size dependence of the transition point for the short range interaction at $\nu = 1/2$.

In the case of the long-range potential the gap Δ may be a strong function of size (see Fig. 3.2) and one should expect a large size effect for relatively small clusters. The only practical way we can propose to estimate the transition point for an infinite crystal is to calculate the energy Δ of the point defect in such crystal and rely upon the criterion Eq. 4.1. Say, for $\nu = 1/2$ we get $\Delta = 0.61$ (see Fig. 3.2) resulting in J_c between 0.28 and 0.41 if we take $0.45 < \beta < 0.68$. Note that to get this number from quantum computations one should consider at least 6×6 cluster with 18 electrons because the point defect becomes the lowest excited state starting from this cluster size (see Fig. 3.2).

Finally, we consider the gap between the split ground state and excited states that belong to the defect band. This gap is clearly seen in Figs. 4.1a,b, 4.3a, and 4.4. At large J the branches have a form of beams with different slopes. These slopes definitely come from the confinement quantization. The large number of states in each beam reflects high degenracy of the free-fermion ground state at $\nu = 1/2$ in the square geometry. Say, in Fig. 4.4 all lines that are horizontal at large J are the state that are degenerate in the free fermion limit. The splitting of these states is the result of interaction. The gap between the split ground state and the bunch of the states in the same beam can be

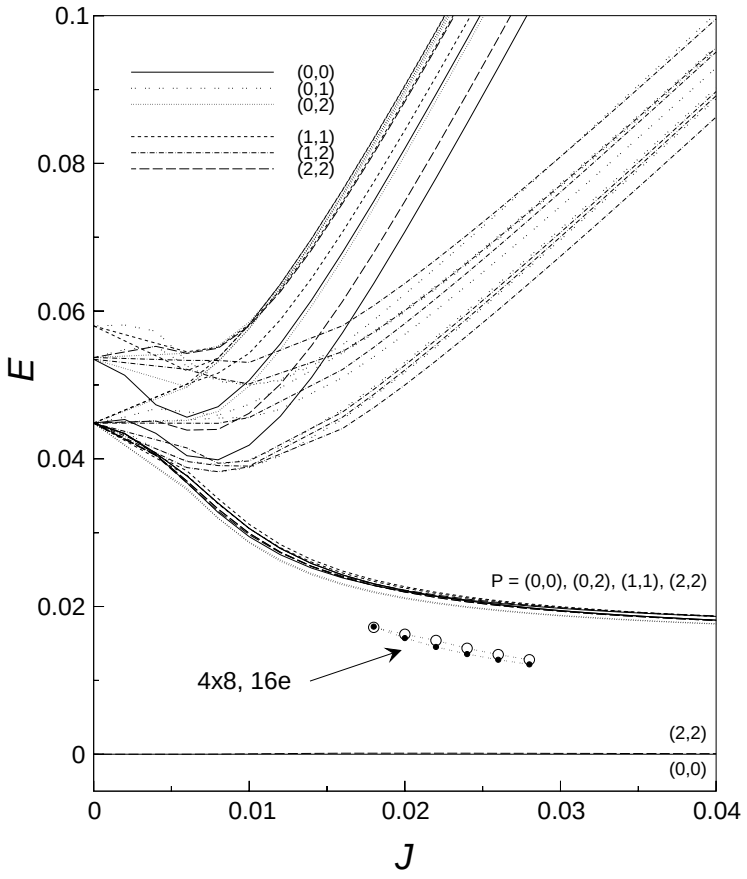

Figure 4.4. The low-energy part of the spectrum for the clusters 4×4 and 4×8 at $\nu = 1/2$. The ground-state energy is used as a reference point. The numbers (n_x, n_y) denote the components of quasimomentum $\mathbf{P} = (2\pi n_x/L_x, 2\pi n_y/L_y)$. The data for 4×8 cluster are presented only for $\mathbf{P} = (0, 0)$ (dots) and $\mathbf{P} = (\pi, \pi)$ (circles).

easily calculated in the mesoscopic region of large J, where $4\pi^2/L^2 \gg 1/L$. The picture of beams is valid in the mesoscopic limit and does not imply the existence of a gap at large J in the macroscopic system.

On the other hand, the gap Δ that appears at $J = 0$ is the energy of point defect and it has a nonzero limit in macroscopic system. Thus, an important question appears; whether or not the gap has a nonzero limit right after the insulator-metal transition. The nonzero gap would mean that the state after the transition is superconducting.

The gap in the transition region is a result of the avoided crossing of the ground state and the defect branch with the same quasimomentum. We have made a lot of computational efforts in this direction but the results are still inconclusive. Our best achievement is shown in Fig. 4.4 where we compare the results for 4×4 and 4×8

clusters. The confinement quantization would prescribe the doubling of the gap. We have found that the gap for the 4×8 cluster is less than for 4×4 cluster but the ratio is significantly less than 2.

CHAPTER 5

RESULTS OF 1D COMPUTATIONS

In this section we would like to check the above picture of the quantum melting in 1D case. The advantage of 1D case is that the size effect can be strongly reduced for the same number of particles.

5.1 1D Coulomb problem

We study the Hamiltonian Eq. 1.1 at filling factor $\nu = 1/2$ and $V(i-j) = 1/|i-j|$. In 1D we switch from the homogeneous background to the chain with $\pm 1/2$ charges for the empty and occupied sites respectively.

The 1D Coulomb WC at $J = 0$ has a structure $\bullet\circ\bullet\circ$, where $\bullet$ stands for an occupied and $\circ$ stands for an empty site. The point defect with the lowest energy is a shift of one electron to the nearest site. It is easy to show that its energy is $\Delta = 2\ln 2 - 1$=0.386. Fig. 5.1 shows the flux sensitivity vs. J for different system sizes L. An extrapolation to $1/L \to \infty$ shown in the inset gives a rather wide interval for J_c between 0.17 and 0.3. This gives for β in Eq. 4.1 the interval $0.44 < \beta < 0.77$. The reason of such a large uncertainity is discussed in the next subsection.

In 1D the picture of the transition can be illustrated by the dependence $E(P)$ at given J. Fig. 5.2 shows the few lowest eigenvalues for each quantized value of P for a system of $L = 28$ sites with $N = 14$ particles. Note that the spectrum has nontrivial symmetry around the points $P = \pm\pi/2$. The states with total quasimomenta P, $\pi - P$, $-P$, and $P - \pi$ are degenerate. This is a general statement for 1D systems with the Hamiltonian Eq. 1.1 for even N at $\nu = 1/2$. The states with quasimomenta P and $\pi - P$ can be obtained from each other by electron-hole transformation $a_p^\dagger \to a_{p+\pi}$.

For even N the WC icon generates two states with quasimomenta $P = \pm\pi/2$, which are degenerate at all J. As one can see form Fig. 5.2, at $J = 0.05$ these states are separated by a gap from the continuum of states, generated by the icon of the point defect. At $J = 0.1$ the defect band becomes wider and the gap decreases as a result.

However, the lowest eigenvalue at $P = \pi/2$ is still a separated point, whereas the second eigenvalue belongs to the defect band. At this point an avoided crossing starts to develop and the width of the gap remains almost unchanged from $J = 0.1$ to $J = 0.2$. In the later case, the lowest eigenvalue is no longer a separated point, but rather can be ascribed to the band. At $J = 0.3$ it becomes absolutely clear that the lowest eigenvalue belongs to the continuum spectrum. Finally, at $J = 1$ the picture is similar to that for free fermions with the fermi momentum $p_F = \pi/2$ and with the lowest branch $E_{min}(P)$ close to $J|\cos(P)|$.

Thus, Fig. 5.2 provides a nice illustration to the mechanism of the quantum melting described in Chapter 3. It shows that the band of the lowest defect plays crucial role in this transition. We think that a similar picture is valid in the 2D case. We do not present

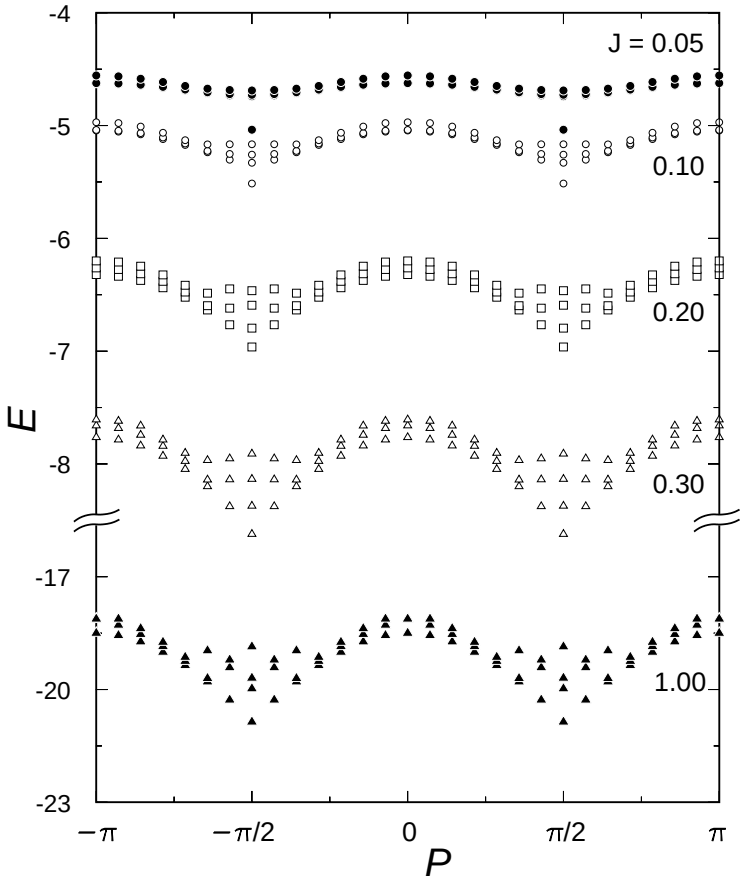

Figure 5.1. The dependence of the total energy on quasimomenum at fixed J for 1D system with Coulomb interaction at $\nu = 1/2$, size $L = 28$.

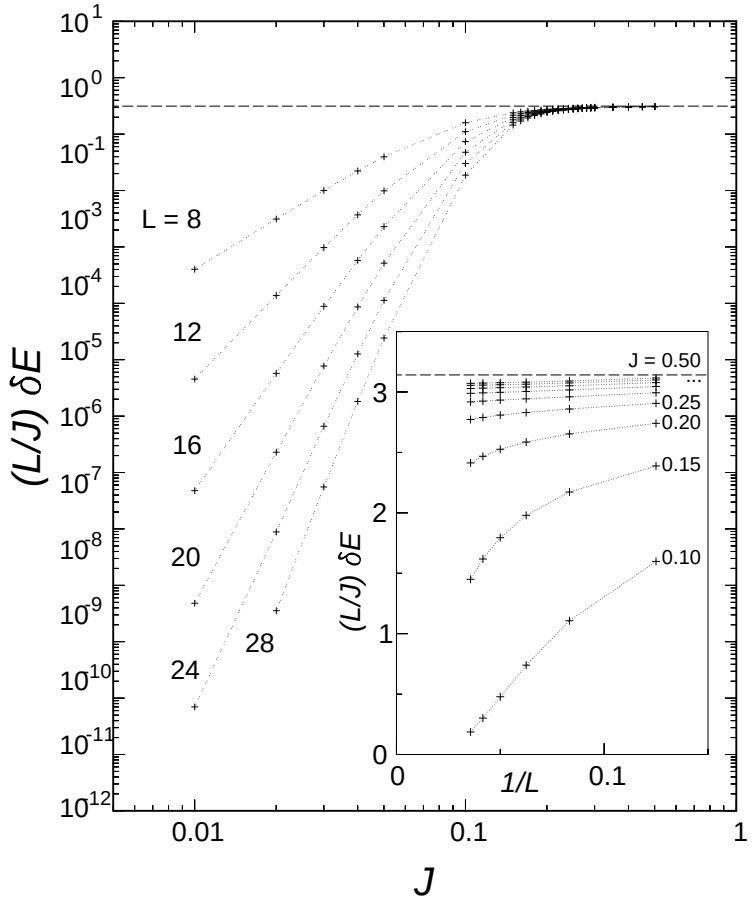

Figure 5.2. Flux sensitivity as a function of J for the 1D system with Coulomb interaction at $\nu = 1/2$ for different sizes L. The inset shows the extrapolation to $1/L \to 0$.

it because for the cluster size available the dependence $E(P)$ does not look so impressive.

5.2 $[V_1, V_2]$-problem

Here we apply the criterion Eq. 4.1 to the 1D problem with the nearest-neighbor interaction V_1 and next-nearest neighbor interaction V_2 at filling factor $\nu = 1/2$. This model is interesting because the gap Δ can be varied in a large interval and can be close to zero at finite V_1 and V_2.

This model has been studied[32] in connection with the spin version of the Hamiltonian Eq. (1.1). The metal-insulating phase diagram for this model has been recently studied in Ref. [33].

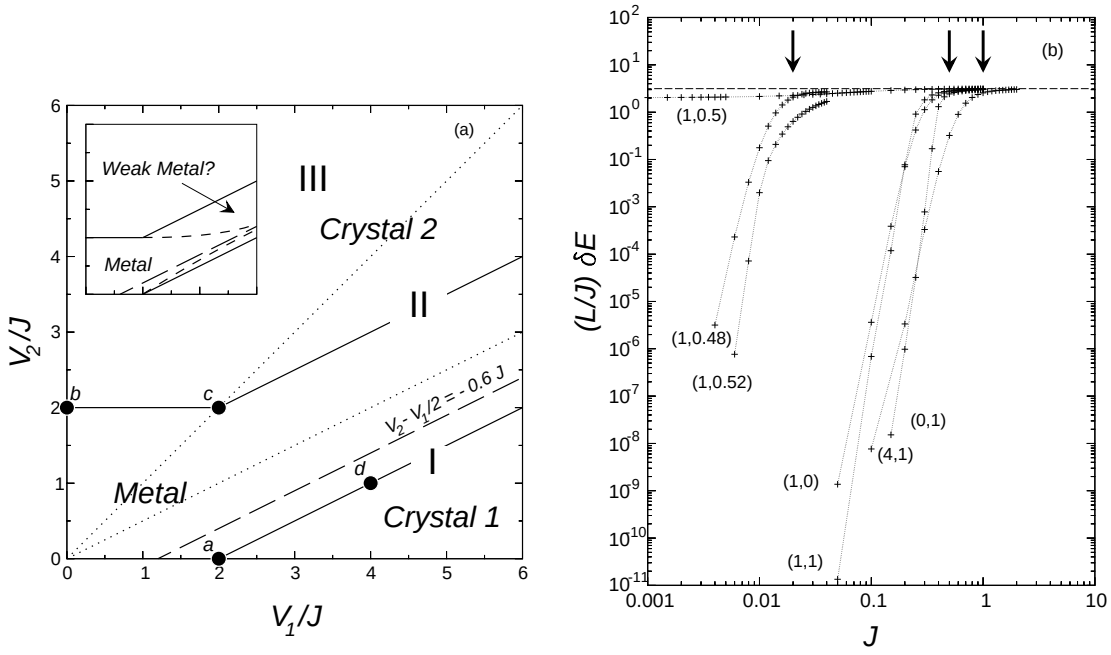

Figure 5.3. The results for $[V_1, V_2]$-model. (a) The phase diagram. Solid lines show the diagram as obtained from Eq. (4). Point a is known exactly; points b, c, and d are checked by computations. The dashed line is the "magic" metallic line. The short-dashed lines in the inset show schematically the boundaries of the normal metallic phase with $L\delta E$ independent of L. (b) The flux sensitivity vs. J for different (V_1, V_2) for the system with 14 electrons. The arrows show the transition points predicted by the phase diagram.

In the $[V_1, V_2]$-model, at $J = 0$, there exist two competing crystals. The Crystal 1 has a structure $\bullet\circ\bullet\circ$. The Crystal 2 is $\bullet\bullet\circ\circ$.

Dotted lines in Fig. 5.3a indicate three regions. Crystal 1 has lower energy in the region I, where $\Delta = 2V_2 - V_1 < 0$. The lowest-energy defect in it has energy $-\Delta$ and represents a shift of an electron to the nearest site. Crystal 2 is stable in the regions II and III, where $\Delta > 0$. In the region II its lowest defect has energy Δ and is also a shift of one electron. In the region III another defect wins, which has energy V_2. This defect is a "domain boundary," when a portion of a crystal is shifted one site to the right or to the left. Such a shift, in fact, produces two domain boundaries simultaneously.

For the exactly soluble problem with nearest-neighbor interaction $\beta = 0.5$. Using this value in Eq. (4.1) one can obtain phase boundaries shown in Fig. 5.3a with solid lines. The lower solid line shows the quantum melting of Crystal 1. The upper solid line shows the melting of Crystal 2. It consists of two straight lines in two different regions, II and

III, which correspond to the melting due to the different types of defects.

Fig. 5.3b shows the results of numerical computation of $L\delta E/J$ as a function of J at fixed V_1 and V_2 for a system of 14 electrons. The data for smaller sizes are not shown. However, they have been used to find the critical value J_c by extrapolation to $1/L \to 0$. At (V_1, V_2) equal to (1,0), (0,1), and (1,1) our criterion predicts the transition at $J_c = 0.5$; at (4,1) it predicts $J_c = 1$. These values are indicated by the points a, b, c, and d in Fig. 5.3a, and by arrows in Fig. 5.3b. The value $J_c = 0.5$ is exact for the point $(1, 0)$[11, 12, 13]. In this case the result of extrapolation gives predicted values for the first three points with a 15% accuracy.[1] For point (4,1) we have $J_c = 1.2 \pm 0.1$. Thus, we may conclude that Eq. (4.1) works very well in the region where Δ is of the order of V_1 and V_2.

The most important statement suggested by the proposed phase diagram in Fig. 5.3a is a prediction of metallic region between the solid lines which extends infinitely for arbitrarily large V_1 and V_2 close to the line $\Delta = 2V_2 - V_1 = 0$. Consider the curves in Fig. 5.3b corresponding to $(V_1, V_2) = (1, 0.48)$ and $(1, 0.52)$. Now with decreasing J we are moving almost along the line $\Delta = 0$ in Fig. 5.3a. In the first case we deviate a little towards the Crystal 1, and in the second case towards the Crystal 2. Both lines intersect the corresponding phase boundaries at large V_1, V_2, predicting $J_c = 0.02$ in both cases. One can see in Fig. 5.3b that this prediction is basically fulfilled in the sense that the exponential dependence on J disappears at this point. For $J > J_c$ the system, however, does not look like an ordinary metal, where $L\delta E$ should be size independent. In fact, we have observed a weak dependence of $L\delta E$ on L in a wide range of J between $J = J_c$ and $J \approx 0.4$.

Fig. 5.3b also shows δE for $(V_1, V_2) = (1, 0.50)$. Now with decreasing J we are moving exactly along the line $\Delta = 0$. In this case the exponential transition to the dielectric phase is absent for arbitrarily small J and for the system size under study, as it follows from our phase diagram Fig. 5.3a. However, there is some size dependence of $L\delta E$ along the line $\Delta = 0$ in the region $J \ll 1$. It can be described as $\delta E \sim 1/L^\alpha$ with $\alpha > 1$. Thus, it is not a regular 1D metal where $\alpha = 1$. In fact, the numerical data can also be consistent with the exponential size dependence $\delta E \propto \exp(-L/\xi)$ with anomalously large correlation length ξ.

---

[1] We claim such a high accuracy for the result of extrapolation because the size dependence looks very similar to the case (V_1, V_2)=(1,0), where exact J_c is known. In the Coulomb case the extrapolation is more uncertain.

Now we study more carefully the close vicinity of the line $\Delta = 0$ far from the origin. In the region $\Delta \ll V_1, V_2$ the spectrum of energies at $J = 0$ has two scales. The large scale is determined by V_1 and V_2, whereas the second scale is $|\Delta|$, that is the energy necessary to produce a defect. When $\Delta = J = 0$ the ground state is macroscopically degenerate.

Below we consider a limit $V_1, V_2 \to \infty$, J and Δ being finite. In this limit the size of the Hilbert space can be greatly reduced. Only the states which are degenerate at $\Delta = J = 0$ need to be taken into account. These states are such that neither three electrons nor three holes occupy adjacent sites.

The reduction of the Hilbert space size is from $C_L^{L/2}$ to approximately f_{L-2}, where f_n denote the Fibonacci numbers, defined by $f_n = f_{n-1} + f_{n-2}$, $f_0 = f_1 = 1$. At large n one has[34] $f_n \approx ((1+\sqrt{5})/2)^{n+1}/\sqrt{5}$.

With this reduction we can increase L up to 40 ($f_{39} = .63 \times 10^8$). Fig. 5.4a shows $\delta EL/J$ as a function of $\Delta/2J$ obtained for different L. The maximum occurs not at $\Delta = 0$, as can be expected from naive consideration, but at $\Delta/2J \approx -0.6$. Accurate size extrapolation shown in Fig. 5.4b demonstrates that at this point $\delta EL/J$ stays finite as L goes to infinity. Thus, the system at $\Delta \approx 1.2J$ is a normal metal. The flux sensitivity in $L \to \infty$ limit is less than the value π for free fermions and is equal $L\delta E/J \approx 2.5$. In the phase diagram Fig. 5.3a the "magic" metallic line $\Delta = 1.2J$ is shown with a dashed line. This line appears, obviously, as a result of quantum mixture of the two different Wigner crystals.

Fig. 5.4a shows also the energy per particle as a function of $\Delta/2J$ obtained in the same limit. We have not found any singularity in the energy in the region of interest. The gap between the ground and the lowest excited states with the same total quasimomentum at the magic metallic line scales to zero linearly in $1/L$, as shown in the inset in Fig. 5.4a. Note that the WC on the lattice has a finite gap.

The inset in Fig. 5.4b shows the reciprocal correlation length $1/\xi = -d\ln(L\delta E)/dL$ as a function of $\Delta/2J$ as obtained from the slopes of the curves in Fig. 5.4b at largest L. Note that the condition $\xi < L$ corresponds to $1/\xi > 0.25$. Thus, we have a real exponential behavior for $-3 < \Delta/2J < 2$. At large negative values of $\Delta/2J$ the ground state of the system is close to the Crystal 2 with a small admixture of defects which are fragments of the Crystal 1. At large and positive $\Delta/2J$ one obtains the opposite picture. In the intermediate region the ground state is a mixture of these two crystals. If we extrapolate $1/\xi$ in each of the exponential regions, we find that it turns into zero

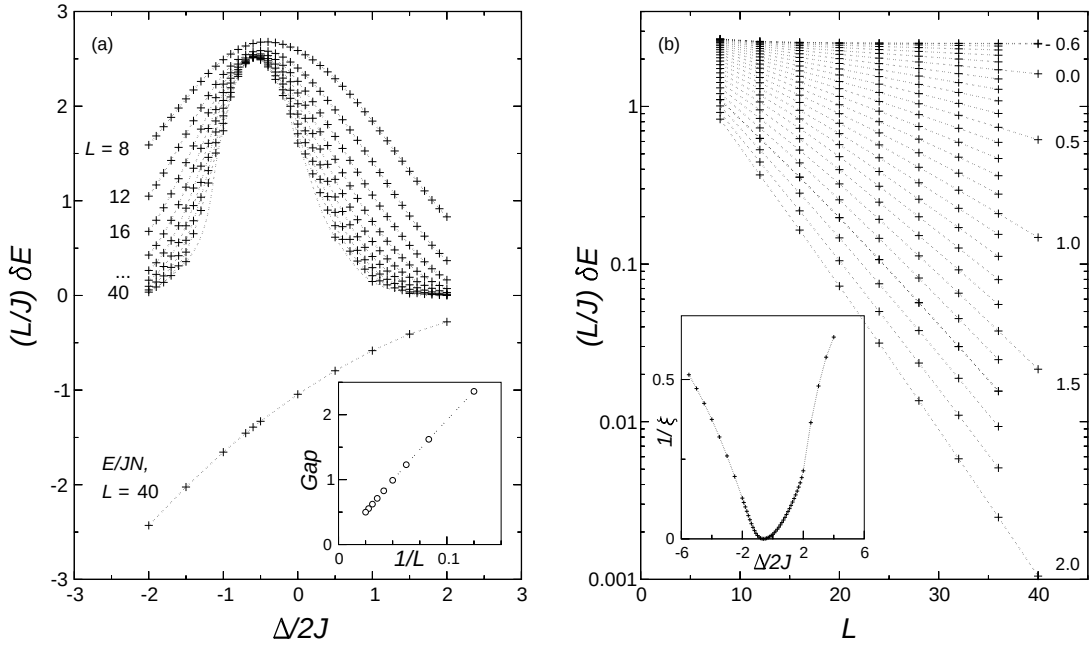

Figure 5.4. Flux sensitivity $L\Delta E/J$ in the limit $V_1, V_2 \to \infty$ vs. $\Delta/2J$ and L as obtained by exact diagonalization. (a) also shows the ground-state energy E per particle vs. $\Delta/2J$ for $L = 40$. The inset in (a) shows the excitation gap at the magic metallic line vs. $1/L$. The inset in (b) shows the slope $1/\xi = -d\ln(L\delta E)/dL$ as obtained from the curves in (b) at largest L. It can be regarded as the reciprocal correlation length when $\xi < L \sim 40$.

approximately at the boundaries of the metallic strip shown in Fig. 9a. This is natural, since the naive picture that leads to these phase boundaries considers quantum melting of a single crystal.

The small value of ξ in the intermediate region suggests that the size dependence of $L\delta E$ is not exponential near the magic line. This would imply the existence of another phase, that may be named a "weak metal." If such a phase exists, there should be a phase boundary which separates the weak metal from the normal metal, where $L\delta E$ is size independent. The inset in Fig. 9a shows schematically the boundaries of the normal metal phase. This diagram is similar to the one obtained in Ref. [33], except it predicts an infinite metallic line in the plane (V_1, V_2).

CHAPTER 6

CONCLUSIONS

We have performed a numerical study of the quantum melting transition of 1D and 2D fermionic systems in a lattice model with Hamiltonian Eq. 1.1. The transition occurs at some critical value of the hopping amplitude J. The structural transition has been detected by studying the splitting of the ground state, degenerate in the crystalline phase. Simultaneously we studied the insulator-metal transition, detecting it by computing the sensitivity of the ground-state energy to the boundary conditions.

We have found out that the quantum melting transition on a lattice is not of the first order. The driving force of the transition is the mixing of the ground-state wave function with the wave function of the point defect in the Wigner crystal. At finite J the point defect forms a band. The melting occurs at such J that the lowest edge of the band comes close to the energy of the ground state. Strong mixing between the crystalline and defect states occurs at this point. This simple picture implies that the critical value of J is determined by the energy Δ of the point defect at $J = 0$. The empirical criterion we have proposed is $J_c = \beta\Delta$, where β is some number.

In the 2D case we have studied the systems with Coulomb and short-range interaction potentials at different filling factors. We have shown that the empirical criterion works very well in all cases studied.

We have shown that the insulator-metal transition occurs simultaneously with the structural transition

We have considered also a 1D lattice model with the nearest-neighbor interaction V_1 and next-nearest neighbor interaction V_2 at filling factor 1/2. This model is interesting because the gap Δ can be varied in a large interval and can be close to zero at finite V_1 and V_2.

We have shown that our criterion provides a good description of the phase diagram of quantum melting in the $[V_1, V_2]$-model in the regions where the mixing of two competing

crystals is not important. In the region of strong mixing we have found an interesting metallic phase in a strongly interacting system.

REFERENCES

[1] A. L. Efros, F. G. Pikus, Solid State Commun. **96**, 183 (1995).

[2] R. Berkovits, Y. Avishai, Europhys. Let. **29**, 475 (1995).

[3] D. L. Shepelyansky, Phys. Rev. Lett. **73**, 2607 (1994); Y. Imry, Europhys. Lett. **30**, 405 (1995);

[4] X. Zhu, S. G. Louie, Phys. Rev. B **52**, 5863 (1995) and early references quoted therein.

[5] E. Dagotto, Rev. Mod. Phys. **66**, 763 (1994).

[6] R. T. Whitlock and P. R. Zilsel, Phys. Rev. **131**, 2409 (1963).

[7] R. T. Scalettar, G. G. Batrouni, A. P. Kampf, G. T. Zimanyi, Phys. Rev. B **51**, 8467 (1995).

[8] A. van Otterlo, K.-H. Wagenblast, R. Baltin, C. Bruder, R. Fazio, G. Schon, Phys. Rev. B **52**, 16176 (1995).

[9] E. Roddick, D. Stroud, Phys. Rev. B **51**, 8672 (1995).

[10] E. S. Sorensen, E. Roddick, Phys. Rev. B **53**, 8867 (1996).

[11] C. N. Yang and C. P. Yang, Phys. Rev. **147**, 303 (1966); **150**, 327 (1966); **151**, 258 (1966), and earlier references quoted therein.

[12] J. des Cloizeaux, J. Math. Phys. **7**, 2136 (1966).

[13] B. Sutherland, B. S. Shastry, Phys. Rev. Lett.**65**, 1833 (1990).

[14] F. G. Pikus, A. L. Efros, Solid State Commun. **92**, 485 (1994).

[15] W. Kohn, Phys. Rev.**133**, A171 (1964).

[16] D. J. Scalapino, S. R. White, and S. Zhang, Phys. Rev. B **47**, 7995 (1993).

[17] M. Buttiker, Y. Imry, and R. Landauer, Phys. Lett. **96**, A365 (1983).

[18] L. P. Levy, G. Dolan, J. Dunsmuir, and H. Bouchiat, Phys. Rev. Lett. **64**, 2074 (1990).

[19] V. Chandrasekhar, R. A. Webb, M. J. Brady, M. B. Ketchen, W. J. Gallagher, and A. Kleinsasser, Phys. Rev. Lett. **67**, 3578 (1991).

[20] D. Mailly, C. Chapelier, A. Benoit, Phys. Rev. Lett. **70**, 2020 (1993).

[21] A. Schmid, Phys. Rev. Lett. **66**, 80 (1991); B. L. Altshuler, Y. Gefen, and Y. Imry, Phys. Rev. Lett. **66**, 88 (1991).

[22] A. Altland, Y. Gefen, and G. Montambaux, Phys. Rev. Lett. **76**, 1130 (1996).

[23] R. Berkovits, Y. Avishai, Solid State Commun. **93**, 301 (1995).

[24] A. L. Efros, E. V. Tsiper, F. G. Pikus, Proc. of 23 Int. Conference on the Physics of Semiconductors, v. **4**, p. 2439 (1996).

[25] H.-F. Cheung, E. K. Riedel, and Y. Gefen, Phys. Rev. Lett. **62**, 587 (1989).

[26] D. Wohlleben, M. Esser, P. Freche, E. Zipper, and M. Szopa, Phys. Rev. Lett. **66**, 3191 (1991); M. Szopa and E. Zipper, Solid State Comm. **77**, 739 (1991).

[27] M. Szopa and E. Zipper, Int. J. of Modern Phys. **9**, 161 (1995); M. Szopa, D. Wohlleben, and E. Zipper, Phys. Lett. **A160**, 271 (1991).

[28] D. Loss and T. Martin, Phys. Rev. B **47**, 4619 (1993).

[29] H.-F. Cheung, Y. Gefen, E. K. Riedel, and W.-H. Shih, Phys. Rev. B **37**, 6050 (1988).

[30] E. V. Tsiper, F. G. Pikus, and A. L. Efros, unpublished, preprint cond-mat/9512150.

[31] L. D. Landau and E. M. Lifshitz, *Statistical Physics*, Part 1, 3rd ed., Pergamon Press, 1980, p. 459.

[32] V. J. Emery and C. Noguera, Phys. Rev. Lett. **60**, 631 (1988); Synthetic Metals **29**, F523 (1989), and earlier references quoted therein.

[33] D. Poilblanc, S. Yunoki, S. Maekawa, and E. Dagotto, preprint cond-mat/9704170.

[34] N. J. A. Sloane *A Handbook of Integer Sequences*, Acad. Press, Boston, 1997.